# Architecture for in-space robotic assembly of a modular space telescope

**Nicolas Lee,[a] Paul Backes,[b] Joel Burdick,[c] Sergio Pellegrino,[a,*] Christine Fuller,[b] Kristina Hogstrom,[a] Brett Kennedy,[b] Junggon Kim,[b] Rudranarayan Mukherjee,[b] Carl Seubert,[b] and Yen-Hung Wu[b]**
[a]California Institute of Technology, Graduate Aerospace Laboratories, 1200 East California Boulevard, Pasadena, California 91125, United States
[b]California Institute of Technology, Jet Propulsion Laboratory, 4800 Oak Grove Drive, Pasadena, California 91109, United States
[c]California Institute of Technology, Department of Mechanical and Civil Engineering, 1200 East California Boulevard, Pasadena, California 91125, United States

**Abstract.** An architecture and conceptual design for a robotically assembled, modular space telescope (RAMST) that enables extremely large space telescopes to be conceived is presented. The distinguishing features of the RAMST architecture compared with prior concepts include the use of a modular deployable structure, a general-purpose robot, and advanced metrology, with the option of formation flying. To demonstrate the feasibility of the robotic assembly concept, we present a reference design using the RAMST architecture for a formation flying 100-m telescope that is assembled in Earth orbit and operated at the Sun–Earth Lagrange Point 2.  [DOI: 10.1117/1.JATIS.2.4.XXXXXX]

Keywords: space telescope; robotic assembly; modular structure; segmented mirror.

Paper 15078SS received Nov. 14, 2015; accepted for publication Jun. 6, 2016.

## 1 Introduction

The aperture size of astronomical telescopes has followed an increasing trend over time to achieve ever-greater light-gathering ability and angular resolution, advancing our scientific understanding of planets, stars, and galaxies, and probing deeper into the universe. Initially limited by the ability to fabricate large monolithic mirrors or lenses, the advent of segmented telescopes and associated wavefront control technologies enabled new ground-based telescopes to be built with apertures on the order of tens of meters in diameter. These telescopes, however, are fundamentally limited by atmospheric distortion and absorption and by their fixed location on the rotating Earth. Space-based telescopes avoid these disadvantages but are subject to additional constraints, including severe limitations on overall launch vehicle volume and mass capacity. Both ground- and space-based telescopes are, of course, also limited by overall cost to justify scientific return.

In this paper, we present an architecture and conceptual design for a robotically assembled, modular space telescope (RAMST) that overcomes these volume and mass limitations, allowing telescope components to be launched incrementally. This capability enables extremely large space telescopes to be conceived, and smaller telescopes to leverage secondary launch payload options, lowering their cost. Our goal here is to address the principal technical challenges associated with such an architecture, so that future concept studies addressing a particular science driver can consider robotically assembled telescopes in their trade space. The principal features of this architecture include a primary mirror constructed using a modular deployable structure, a general-purpose robot to assemble the telescope and be available for subsequent servicing tasks, and advanced metrology technologies to support the assembly as well as wavefront control during operation. An additional optional feature included in the architecture is the possibility of formation flying the separate components of the telescope. This particular combination of features provides a system architecture that is scalable to a wide range of telescope sizes and is not limited to a particular optical design.

A particular telescope configuration that is presented in this paper is a five-mirror $F/4$ telescope including a 100-m spherical primary mirror and four mirrors in a spherical aberration corrector, as shown in Fig. 1, with intended operation around the Sun–Earth Lagrange Point 2 (SEL2), as a successor to the James Webb Space Telescope (JWST) and the High Definition Space Telescope (HDST) concept.[1,2] A telescope of this size exceeds the capacity of currently existing or proposed launch vehicles and would require at least four heavy lift launches (such as the SLS Block 1B) to transport all components to orbit. The large dimension of the optical elements and the benign gravitational environment at SEL2 motivate partitioning the telescope system into four formation-flying components: the primary mirror, the optics and instrumentation unit (OIU), the metrology unit, and a sunshade. Each of these four components is a stand-alone spacecraft mechanically isolated from the others. The OIU contains the spherical aberration corrector and a wide-field-of-view finder telescope as well as instrumentation and a high-gain communications system for transfer of scientific data and images. The metrology unit contains a laser metrology system that incorporates multiple technologies providing the required dynamic range and precision for assembly and operation.

The primary mirror itself includes a layer of identical hexagonal deployable truss modules (DTMs), each supporting one mirror module holding multiple mirror segments. Individual mirror segments are mounted on a rigid body actuator platform within the mirror module. Figure 2 shows the national assembly

*Address all correspondence to: Sergio Pellegrino, E-mail: sergiop@caltech.edu

2329-4124/2016/$25.00 © 2016 SPIE

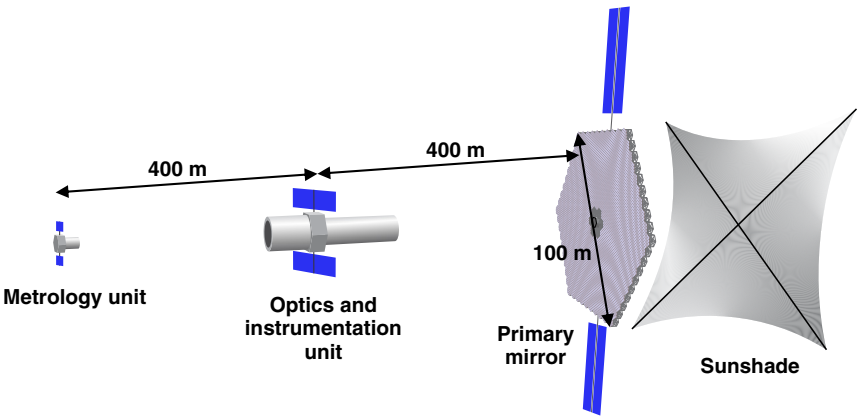


**Fig. 1** Artistic depiction of formation flying 100-m telescope configuration (distances between components are not to scale).

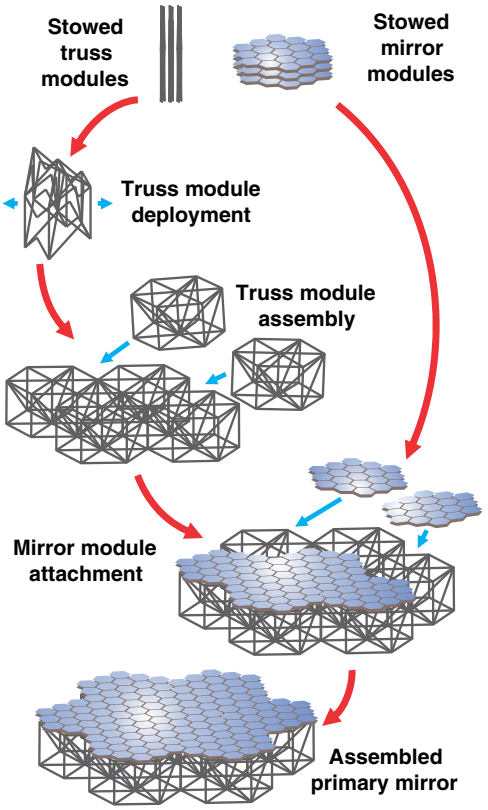


**Fig. 2** Primary mirror assembly concept and module nomenclature.

sequence for a set of three truss and mirror modules. First, the truss modules are individually deployed and attached. Once the structure is complete, the mirror modules are attached to the underlying truss. A full 100-m primary mirror includes over 300 of each module, requiring numerous repetitive manipulation tasks suitable for a robotic system with supervised autonomy.

The primary mirror assembly is performed by a general-purpose robot that will remain with the telescope and that will also perform servicing tasks throughout its lifetime. This robot, shown in Fig. 3, is a multilimbed robot that can travel over the primary mirror truss structure to perform its assembly and servicing tasks. These tasks include transporting truss and mirror modules across the partially assembled primary mirror

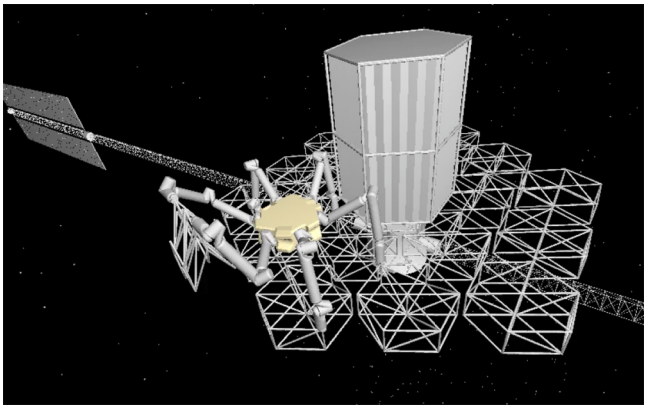

**Fig. 3** Conceptual CAD rendering of assembly robot deploying a truss module. Folded truss modules are stored in a cargo housing unit shown docked to the central hub. Accessibility of the folded modules is subject to future detailed design.

structure, positioning and aligning the modules for assembly, and removing and installing components, such as individual mirror segments for servicing.

The following section summarizes prior work related to the RAMST architecture, including a comparison with some of the many concepts developed for large-space telescopes. Section 3 provides an overview of the features and advantages of the RAMST concept and presents some of the trade studies considered. Section 4 explores the 100-m telescope configuration in detail, including the optical, metrology, and structural designs. Section 5 describes the robotic system and assembly sequence. Section 6 summarizes and concludes the paper.

## 2 Background

The RAMST architecture builds upon substantial prior work in order to enable aperture diameters on the order of 100 m to be assembled in space. Such large diameter telescopes operating in the UV to near IR wavelengths would enable significant science return in characterizing terrestrial exoplanets and stellar populations, understanding galaxy halo and gas physics, and studying dark matter dynamics.[3,4] Here, we briefly summarize prior large telescope designs and in-space assembly techniques that provide context for the development of the RAMST architecture.

### 2.1 *Large Ground- and Space-Based Telescopes*

The largest monolithic reflecting mirrors constructed for ground-based astronomical telescopes are 8.4 m in diameter, used in the Large Binocular Telescope and also being fabricated for the Giant Magellan Telescope.[5] Starting with the two 10-m Keck telescopes[6] completed in the 1990s, large observatories have relied on segmented mirrors to achieve even larger aperture sizes. Most recently, the Thirty Meter Telescope and the European Extremely Large Telescope are planned to have apertures of 30 and 39.4 m, respectively, with primary mirrors composed of 492 and 798 hexagonal segments.[7,8] The Hobby–Eberly Telescope and South African Large Telescopes are designed for spectroscopic measurements rather than imaging, and use 11-m spherical primary mirrors composed of 91 segments each.[9,10] The spherical geometry drastically simplified the mirror fabrication process, resulting in a total cost that is about 20% of a similarly sized general-purpose telescope. The Overwhelmingly Large Telescope concept also used a spherical geometry for its proposed 100-m primary mirror to provide a feasible path for mirror fabrication.[11] Space-based observatories have likewise progressed, from the Hubble Space Telescope (HST) with a 2.4-m monolithic mirror to the Herschel infrared space telescope with a 3.5-m monolithic mirror, and now to the JWST with a 6.6-m deployable mirror composed of 18 segments.[1] To accommodate the payload volume constraint of the Ariane 5 rocket, the backplane truss of the JWST is separated into three hinged sections such that the primary mirror can be folded for launch.

There exist many proposed concepts for future space telescopes larger than the JWST, including three configurations from the Advanced Technology Large-Aperture Space Telescope (ATLAST) study ranging from 8 to 16 m,[3] the 11.7-m HDST,[2] annular 20 to 30 m telescopes using a bicycle wheel structure,[12,13] and the Membrane Optical Imager for Real-time Exploitation (MOIRE) 20-m telescope that uses membrane diffractive optics.[14] However, these particular telescope configurations are fundamentally constrained by the available capacity on a single launch vehicle. Several other telescope concepts, described below, have been proposed that rely on in-space assembly, relaxing this particular constraint.

### 2.2 *In-Space Assembly*

In-space assembly using astronauts and robots has been studied extensively since the 1970s,[15,16] including construction activities tested in a laboratory, in a neutral buoyancy facility, and in space. The construction of the International Space Station (ISS) relied on a combination of tasks using astronauts and teleoperated robotic elements. This capability required the design of new mechanical interconnects to facilitate alignment and latching between truss modules[17] as well as techniques for robotic operation.[18] The HST servicing missions could be considered an example of astronaut-assisted construction tasks associated with a space telescope.[19] At a smaller scale, the Autonomous Assembly of a Reconfigurable Space Telescope spacecraft, currently under development, will demonstrate autonomous reconfiguration of a modular space telescope using microsatellites.[20]

Conceptual designs for space telescopes assembled in space include a robotically assembled 20-m telescope launched with an associated robot[21] or brought to the Space Station for assembly,[22] the filled aperture infrared telescope/dual anamorphic reflecting telescope 10 m concept assembled by astronauts at the Earth–Moon L1 point,[23] an autonomously assembled 10-m telescope,[24] a 30-m telescope assembled by robots at the Earth–Moon L2 point and subsequently transported to the Earth–Sun L2 point, and a modular 20-m telescope with a variety of possible assembly options and locations.[4]

## 3 Features and Advantages of the Robotically Assembled, Modular Space Telescope Architecture

As discussed earlier, the distinguishing features of the RAMST architecture compared with the concepts summarized above include the use of a modular deployable structure, a general-purpose robot, and advanced metrology, with the option of formation flying. Each of these features individually yields benefits in terms of cost or performance, but in combination, the advantages are much more significant.

### 3.1 *Modular Deployable Structure*

The configuration of the backplane structure can be achieved through a combination of deployment and assembly, with options ranging from a single deployable structure to assembly of individual truss members and nodes. The RAMST approach is to include a balance of both deployment and assembly, avoiding the disadvantages of purely deployable or purely assembled structures. A detailed discussion of the backplane for the 100-m reference configuration is presented in Sec. 4.3.

In the case of a single deployable structure, the 16.8-m ATLAST concept[3] is near the upper limit for a fully filled aperture. Telescopes beyond this size would likely exceed the payload capacity of existing and proposed launch vehicles. Even deployment of the supporting backplane structure alone without the reflecting surface would present a substantial challenge because of the numerous mechanisms (e.g., hinges, telescoping tubes, latches, and so on) that must actuate without jamming and in the correct sequence.[25] Ground-based testing of large deployable structures prior to flight is also complicated by the difficulty of gravity offload.[26]

Linearly deploying structures have been demonstrated on a length scale appropriate to large telescopes. The Folding Articulated Square Truss Mast (FASTMast) has been used to deploy the 35-m long solar array wings of the ISS,[27] and the able deployable articulated mast was used to deploy the Shuttle Radar Topography Mission instrument to a distance of 60 m[28] and the NuSTAR optical package to a distance of 10 m.[29] Two-dimensional deployment at this length scale has been demonstrated for membrane and mesh surfaces but not for precision truss structures as required by optical reflectors. An example of a demonstrated membrane deployment is the IKAROS solar sail, which deployed a $14 \times 14$ m solar sail with integrated solar cells using centrifugal forces.[30] Unfurlable mesh reflector antennas for Ka-band, with surface precision of 0.3 mm RMS, have been produced that are up to 9 m in diameter, as well as lower precision antennas up to 22 m in diameter.[31,32] Two modular deployable mesh reflectors, each with an effective aperture of 13 m and composed of 14 basic modules, were flown on the ETS-VIII mission.[33] As discussed in Sec. 2.1, sparse aperture or membrane telescopes at the 20 to 30 m scale have been proposed as single deployable systems. However, in-space assembly tasks become essential

when considering even larger telescopes, or even fully filled reflectors at the 20 to 30 m scale.

On the opposite end of the spectrum, the backplane can be assembled from separate nondeployable elements. Constructing a backplane truss structure from nodes and struts can involve thousands to tens of thousands of operations, depending on the size of the reflector. Assembly techniques by astronauts have been tested in simulated 0-g (underwater) and in space for structures with up to 315 struts.[15] Specialized joints were designed to minimize hand motions and the use of tools, but astronaut fatigue was identified as a limiting factor for assembly of larger structures. Robotic assembly was demonstrated for a truss structure composed of 102 struts and covered with 12 panels, taking ~20 h to complete.[16]

With the RAMST approach of assembling easily deployed modules, the number of assembly tasks can be reduced by 1 to 2 orders of magnitude, while avoiding the challenges and limitations of a monolithic deployable structure. Additionally, if the modules can be designed to be identical, this would greatly simplify the ground-based manufacturing and verification tasks and allow for greater robustness to individual deployment failures through the inclusion of a limited number of spare modules.

### 3.2 *Robotic System*

A detailed discussion of the robotic system for the 100-m reference configuration is presented in Sec. 5. In general, the robotic system involved in the assembly is expected to perform manipulations that involve gross movement of components and make connections using specially designed structural and power interconnects. The robot is also expected to move across the evolving telescope structure in order to carry components from the storage canister attached to the spacecraft to the location of assembly, and to optimally position itself for key assembly tasks.

Examples of the different robotic architectures considered for the assembly task include free-flying systems with two limbs, a wheeled robot that moves on rails on the structure being assembled, and a multilimbed robot that walks on the trusswork. Multirobot co-operation[34,35] is an alternative to the single-robot approach we describe here, but our analysis determined that the cost of the extra communication, sensing, and complex software needed to robustly enable such co-operation outweighs the small benefits to be gained by the use of multiple robots to manage transportation and assembly tasks. The multilimbed single-robot option was chosen as the preferred architecture as it best met the different expectations for the robotic system. Such a robot would be actuated using electric motors and hence could draw power directly from the telescope's solar grid without requiring consumable fuel for propulsion. It could walk on the trusswork using some or all of its multiple limbs without requiring special structural elements (e.g., rails) for mobility. If each limb can be used both as an arm to manipulate and grasp truss elements, and also as a leg for locomotion over the truss structure, then a six-limbed design meets mobility and manipulation requirements. With six limbs, four limbs can be dedicated to locomotion across the truss (using a wave gait in which at least three legs securely grasp the truss), while two limbs secure a module for transportation. While it is not carrying loads or engaging in manipulation, a six-legged design can use a tripod gait to facilitate more rapid traversal of the truss, while maintaining three attachments to the truss at all times. For assembly, three of the limbs could be used as anchors to attach to the trusswork while using the remaining limbs for manipulation. The robot would also be able to carry loads on its base without impeding mobility. Further, such a robot would have sufficient degrees of freedom (DOF) to accommodate and reduce interaction loads with the trusswork and to control internal forces within the robot-truss mechanism.[36] The larger number of DOF in such a robot can also be used to minimize the displacement of the robot's center of mass during locomotion or manipulation tasks,[37] thereby minimizing perturbations to the structure from the robot's operations.

### 3.3 *Advanced Metrology*

An advanced metrology system is included in the RAMST architecture to perform two tasks. First, it serves the purpose of a co-ordinate measuring machine to provide proper alignment between modules during assembly. Second, it provides surface figure measurements for dynamic wavefront control during operation of the telescope. To achieve these tasks, the metrology system requires a wide spatial dynamic range, wide spatial and temporal bandwidths, and must provide simultaneous measurement across the full aperture. A set of technologies that can satisfy the metrology requirements for the 100-m reference configuration is presented in Sec. 4.2.

In general, the RAMST architecture requires a wide spatial dynamic range that spans from centimeter-level positioning of modules as they are manipulated by the robot, down to nanometer-level precision for optical or ultraviolet wavelengths. Spatial and temporal bandwidths also need to be wide, ranging in length from segment-level displacements with length scales on the order of 10 to 100 cm up to full-aperture modes with length scales on the order of 10 to 100 m, and in time from structural vibrations with periods on the order of seconds up to orbital loads (e.g., thermal, gravitation) with periods on the order of hours to days.

In order to provide wavefront control during operation, the metrology system must be capable of simultaneous measurement across the full aperture without repointing the telescope. Interferometric techniques such as with a laser tracker[38] are typically used, with six point measurements per segment to solve for rigid body displacement (three translational and three rotational DOF) and an additional three per segment to account for thermal expansion. However, such a point measurement system, or a distributed metrology system, is infeasible for a telescope with hundreds or thousands of individual mirror segments. At this scale, a centralized metrology system is required that can simultaneously track the state of all mirror segments across the aperture.

To span this entire range, a layered metrology system is needed that combines coarse measurements on a large absolute scale with fine measurements over a shorter relative scale.[39] The coarse measurements would be included in the robot assembly control loop as well as to maintain alignment of secondary optics with the primary mirror. After the coarse measurements establish the optical surface figure to a prescribed threshold, the fine measurements can be used to maintain diffraction-limited performance through the control of active optics.

### 3.4 *Formation Flying of Secondary Optics*

As telescopes increase in size, a greater proportion of the total system mass must be allocated to the supporting structure to

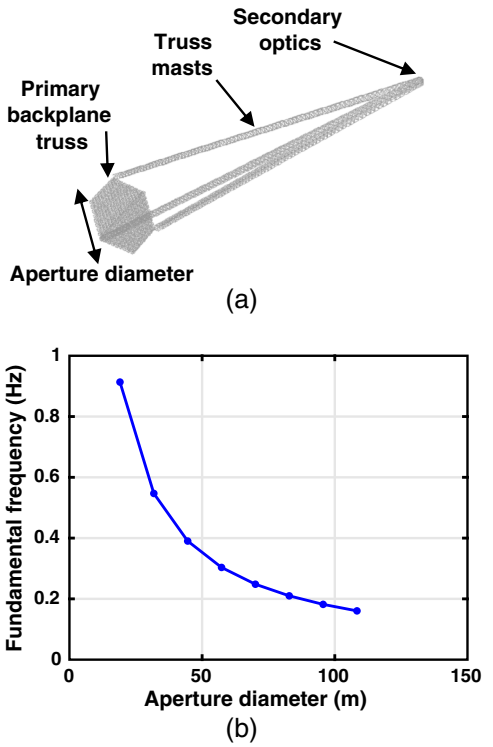


**Fig. 4** Fundamental frequency for structurally connected telescope as a function of aperture size.

maintain alignment of the optical system. Alternatively, concepts have been proposed for flying telescope components as separate spacecraft in formation, using feedback control to maintain system accuracy, instead of structural rigidity. The use of formation flying for the 100-m reference configuration is discussed in Sec. 4.4. Free-flying distributed spacecraft telescopes and interferometers have been investigated in detail with proposed missions including Terrestrial Planet Finder,[40] Stellar Imager,[41] and external occulters with the Telescope for Habitable Exoplanets and Interstellar/Intergalactic Astronomy[42] and New Worlds Observer (NWO).[43] These require the additional mass of independent spacecraft systems for propulsion, communications, and power, but can scale to larger telescope configurations without the increase in mass required for connecting and maintaining alignment of the individual components. Guidance and control algorithms needed for autonomous and precise spacecraft formation flight have been demonstrated, including ground-based demonstrations in JPL's Formation Control Testbed,[44,45] through applications such as starshade missions.[46]

On-orbit demonstrations of autonomous formation flight have also been successfully achieved with the Prisma mission,[47] the TerraSAR-X add-on for Digital Elevation Measurement (TanDEM-X) mission,[48] with CubeSats,[49] within the confines of the ISS on the Synchronized Position Hold Engage Re-orient Experimental Satellites (SPHERES) testbed,[50] and achieving science with the upcoming external coronagraph Proba-3 mission.[51]

Depending on the telescope size and the orbital environment, formation flying may be required or may be infeasible. To identify the limiting size above which formation flying is needed, we used a finite-element analysis to study the effect of increasing telescope size on structural stiffness. A reference design was selected for an $F/4$ telescope configuration with three truss masts extending from the edge of the primary mirror to the location of the secondary optics at the focal point. The truss masts were sized to have diameters that are $1/20$ of the aperture diameter to limit occlusion of the primary mirror. Figure 4(a) shows the geometry of the finite-element model and Fig. 4(b) shows the fundamental frequency of the telescope truss structure including primary backplane and masts, as a function of aperture diameter. For telescope designs with aperture greater than 19 m, the fundamental frequency is less than 1 Hz, which is a threshold corresponding to structural deformations exceeding the limits of a typical control system. This threshold suggests that telescopes larger than 19 m would be more suited to a formation-flying configuration for the secondary optics.

Several additional advantages are provided by a formation flying architecture. Some external disturbance forces can be decoupled from the optical system, such as much of the solar radiation pressure (SRP) and thermal cycling, by physically separating the sunshade system from the primary mirror. The total propulsion requirements, discussed in more detail in Sec. 4.4.3, may be reduced by allowing small slewing maneuvers, where a spacecraft containing the secondary optics moves relative to a fixed primary mirror. This is possible if the primary mirror is spherical and would avoid the requirement for precise rotation of much of the total system mass.

## 4 Reference Design for 100-m Telescope

In this section, we present a reference design using the RAMST architecture for a formation flying 100-m telescope that is assembled in Earth orbit and operated at SEL2. The choice of a 100-m design was chosen to provide a particular example demonstrating the feasibility of the robotic assembly concept at a scale larger than is achievable through other architectures, such as deployment of a telescope from a single launch. However, as outlined in Sec. 3, the concepts presented here are suitable for a wide range of telescope configurations both larger and smaller than this 100-m reference design. The following subsections provide specific details on the optical, metrology, structural, and formation flying architecture of the 100-m telescope, as well as the space environmental conditions that must be considered.

### 4.1 *Optical Design*

A number of telescope configurations were considered, including a Richey–Chretien, several three-mirror anastigmat variations, and a spherical primary with spherical aberration corrector. The spherical primary mirror configuration was most attractive in this trade space because it includes only one large mirror that would require assembly, while the remaining optical elements occupy a compact volume that can be launched as a single unit contained by the OIU spacecraft. The field of view for this design is 4.2 arc min within a field of regard of 1.84 steradian (corresponding to a 90-deg cone aligned away from the sun).

The optical layout of this reference design is a five-mirror configuration including a spherical primary mirror (M1) that has a 100-m diameter and 800-m radius of curvature, as shown in Fig. 5. The four subsequent mirrors (M2 to M5) housed in the OIU form a spherical aberration corrector and include a deformable mirror (M5) for fine wavefront control. Additionally, a small-diameter but wide-field-of-view finder telescope is aligned along the optical axis to aid in slew maneuvers of the OIU. This finder telescope (composed of mirrors

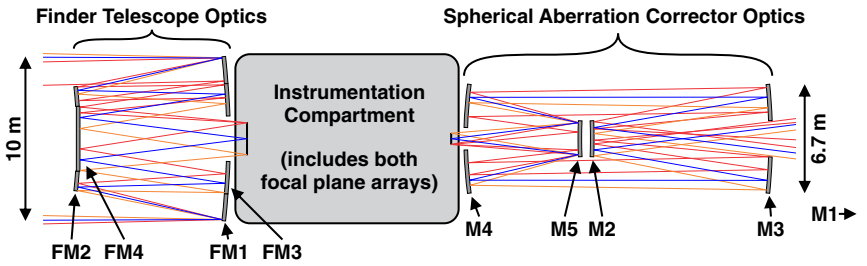


**Fig. 5** Optical layout of the OIU containing the finder telescope and the spherical aberration corrector of the science telescope, with representative ray traces for both telescopes.

FM1 to FM4 in Fig. 5) uses a short focal length design similar to the three-mirror Space Surveillance Telescope[52] but with an additional flat mirror (FM4) to position the focal plane on the side of the telescope connected to the spacecraft chassis. Instrumentation is located in a compartment between the spherical aberration corrector and the finder telescope within the OIU spacecraft chassis.

In order to provide diffraction-limited imaging performance, the telescope uses two-stage optics[53] and adaptive secondary techniques[54,55] to correct for wavefront errors introduced in the primary mirror, avoiding the need for actuators that can achieve nanometer-level alignment of the primary mirror segments. These techniques require a metrology system that can simultaneously track displacements of all primary mirror segments to a precision of several nanometers over a range of centimeters, so that a highly actuated deformable mirror at the exit pupil can undo the rigid body motion of the primary mirror segments and correct for figure distortions. A potential metrology system is described in Sec. 4.2, and the exit pupil mirror can be implemented using technologies, such as a silicon carbide or carbon fiber reinforced polymer deformable mirror using a surface-parallel actuator array.[56,57]

Table 1 summarizes the geometry of the five mirrors that form the main telescope. The primary mirror is composed of 5016 hexagonal segments with a side length of 0.675 m, as shown in Fig. 6. The segment size was chosen to be compatible with existing production facilities for silicon carbide mirrors.[58,59] However, for such a large number of identical mirrors, we envision that a specialized facility would be justified for their manufacture and calibration. These mirror segments are clustered into 264 quasihexagonal modules of 19 segments each, corresponding to the underlying truss backplane described in Sec. 4.3. Mirror modules consist of clusters of mirror segments mounted on a thin plate that provides electrical and mechanical interfaces to the supporting backplane structure. Each mirror segment is mounted on this supporting plate through actuators that provide rigid body tip, tilt, and piston motions for correcting static or slowly varying disturbances. The size of these modules, with a maximum dimension of 6.3 m, was chosen to fit within the proposed Space Launch System (SLS) Block 1B 8.4 m fairing, which has an internal payload envelope diameter of 7.5 m.[60] Alternatively, a larger module of 37 segments would have a maximum dimension of 8.8 m, requiring the use of the 10 m fairing proposed for SLS Block 2B. A smaller module of seven segments with a maximum dimension of 3.8 m would be compatible with existing 5-m fairings. The 7-, 19-, and 37-segment options would include a total of 702, 264, and 120 modules, respectively, to provide a 100-m aperture with 20% diameter central obscuration. Within the OIU, the two smaller mirrors (M2 and M5) have a diameter of 2 m while the larger mirrors (M3 and M4) are segmented and have an aperture diameter of 6.7 m. Figure 7 shows a possible segmentation of M3 and M4 using three rings of hexagonal mirrors with 0.4 m side length.

In order to maintain a cost-effective fabrication and ground-based verification and validation process, a high degree of geometric commonality is included in the design. Specifically, all of the primary mirror segments are identical in both surface figure and hexagonal shape, and each module of 19 segments is arranged identically with two rings of segments around a central

**Table 1** Mirror parameters in scientific telescope.

| Mirror | Aperture diameter (m) | Nominal ROC (m) | Number of segments | Actuation |
|---|---|---|---|---|
| M1 | 100 | 800 (concave) | 5016 | Rigid body segment position |
| M2 | 2.0 | 28.9 (convex) | 1 | Not applicable |
| M3 | 6.7 | 29.3 (concave) | 54 | Not applicable |
| M4 | 6.7 | 22.4 (concave) | 54 | Not applicable |
| M5 | 2.0 | 22 (convex) | 1 | Surface-parallel array |

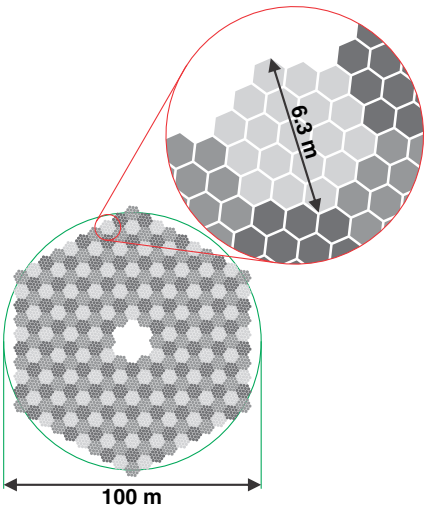


**Fig. 6** Primary mirror (M1) configuration with 264 mirror modules and 5016 mirror segments, with close-up of one module containing 19 segments.

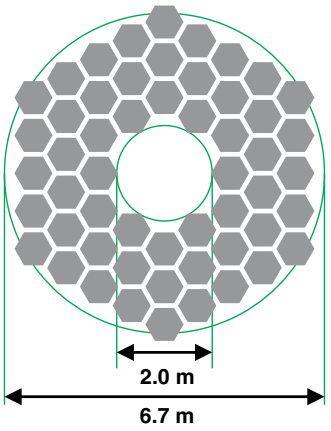


**Fig. 7** Segmentation of the SAC M3 mirror, with a similar arrangement for M4.

segment. Additionally, an average gap width between segments of 100 mm was imposed in order to allow for robot mobility during and after assembly. However, segmentation of the primary mirror surface into identical hexagons is a nontrivial problem because of the effect of variable gap width between segments. These gaps have an impact on the optical performance of the telescope and on the geometry of the backplane structure. Given the constraints described above, the mirror segments were positioned based on the azimuthal equidistant centroid tiling (AECT) method, achieving a maximum absolute deviation in gap width of 2 mm from the nominal 100 mm.[61] The gaps range from a minimum of 98 mm to a maximum of 101.3 mm, with variations of no more than 1.7 $\mu$m between segments within the same module. This arrangement of segments and module positions could be further improved using numerical optimization techniques. With the inclusion of actuators to enable piston, tip, and tilt correction of each individual mirror segment, the total thickness of a mirror module is expected not to exceed 0.3 m. The structural backplane supporting the mirror segments is discussed in Sec. 4.3.

The use of identical segments and modules is essential in this scale of telescope not only for factors associated with manufacture but also for robustness to possible failures during assembly and operation. With identical segments, a small number of spares can be launched and stored on the telescope to replace any segments that incur damage. By contrast, an equivalent primary mirror using uniquely shaped segments in either outline or surface figure would require a large number of spare parts.

### 4.2 *Metrology Architecture*

As discussed in Secs. 3.3 and 4.1, diffraction-limited performance of the telescope necessitates a metrology system that has high spatial precision over a wide range and over a wide temporal bandwidth. An implementation that can achieve this performance includes layers of different technologies to span the required measurement regimes. A centralized laser metrology system was selected, using a laser source that is located at the center of curvature of the primary mirror, at a distance of 800 m from the primary and 400 m from the OIU. This architecture is similar to the interferometric test tower used in the manufacture of monolithic 8.4 m mirrors.[38,62]

Three technologies using this centralized laser source provide a possible metrology architecture that satisfies the requirements for telescope assembly and operation. These include an absolute metrology technique using a modulated dual-frequency laser, dynamic Zernike wavefront sensing for coarse mirror phasing, and array heterodyne interferometry (AHI) for fine phasing. Additionally, a Shack–Hartmann wavefront sensor could be used to complement the above sensors by providing a measurement of wavefront gradient.

The Modulation Sideband Technology for Absolute Ranging (MSTAR) technique has been demonstrated to achieve absolute metrology with better than 10-$\mu$m precision over a 10-m distance and can be extended to the required 800-m range.[63] The basic principle of MSTAR is to use the shift in phase of the fundamental laser frequency to obtain a precise distance measurement and to solve for the phase ambiguity using a sideband frequency introduced by modulating the laser output. The modulation can be designed to provide a sideband frequency that is precise enough to capture every integer phase solution so that the measurement range is continuous. This measurement provides feedback to the robotic system as the primary mirror is assembled and to the formation flying control system during both assembly and operation.

Dynamic Zernike wavefront sensing provides a measurement of wavefront phase at an input pupil by introducing a dynamic and variable phase shift to the central core of a point spread function (PSF), resulting in a mapping to the image intensity at the output pupil.[64,65] This phase shift can be introduced at the metrology laser source using a piezoelectric actuator. The measurement can be used to initialize the phase correction process by providing feedback to the segment rigid body actuators and to occasionally refresh the phasing maintenance from drift due to slowly varying disturbances. To measure the piston and phase step between two neighboring primary mirror segments, we require the phase delay of the PSF core to be dynamically controlled over $\pm 50$ wavelengths. This can be implemented using an all-reflective optical assembly to allow operation across the UV to near IR wavelengths of interest.

Finally, AHI[66] provides fine wavefront measurement to provide feedback to the active exit-pupil mirror so that it can correct for residual distortion in the primary mirror. Compared to distributed metrology architecture, the centralized AHI system allows the full aperture to be measured simultaneously while using a single laser source, reference fiducial, and focal plane array. The use of an aerial sensor avoids the need for individual point measurements for each segment, which is at least three times the number of segments in order to recover the rigid body displacements relative to a desired spherical reference surface. Additionally, the measurements can be taken without having to perturb the segments, unlike dispersive wavefront sensor or phase retrieval methods.[67,68]

### 4.3 *Modular Structural Design*

The main structural challenge for the 100-m formation-flying telescope is the construction of the backplane for the primary mirror. This structural element must accommodate the spherical geometry of the primary mirror surface, provide adequate stiffness to satisfy the optical error budget, and be amenable to high volumetric compaction for launch. To achieve these requirements, we partition the primary mirror backplane into a layer of identical, DTMs corresponding to the mirror modules described in Sec. 4.1. Several DTM configurations were considered, including cubic, hexagonal, and tetrahedral–octahedral trusses. We selected the hexagonal Pactruss configuration as

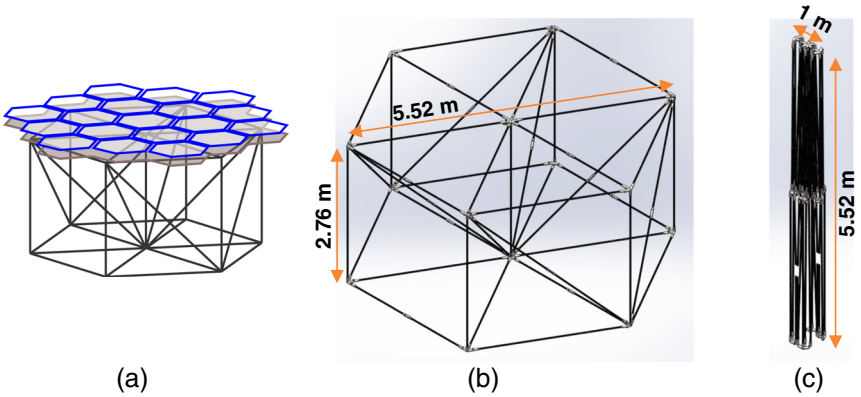


**Fig. 8** (a) Geometry of a single truss module underneath a mirror module; (b) CAD model of deployed truss module; and (c) CAD model of packaged truss module.

the design for each DTM because of the existing prior work in establishing the mechanical configuration for packaging and deployment,[25,69] and because the hexagonal shape is most compatible with the mirror segment geometry. Figure 8 shows one truss module with its associated mirror module attached.

Using the hexagonal tiling pattern established by the mirror module geometry in Fig. 6, there are two possible underlying tessellations that the truss structure can utilize. As shown in Figs. 9(a) and 9(b), these are a fully filled hexagonal tessellation and a sparse tessellation composed of hexagons with triangular voids. We chose to adopt the sparse tessellation for several reasons. Most importantly, the sparse geometry includes fewer redundant truss members compared to the fully filled hexagonal tessellation, as seen in Figs. 9(c) and 9(d), and allows the assembly robot more access and maneuvering space during the assembly operation to manage the process of joining connectors and mating the truss modules. Additionally, the orientation of each truss module is consistent; while in the fully filled case, they must alternate which side faces upward and therefore must include two different DTM configurations for interconnects and mirror attach points. Finally, the hexagons in the sparse case are 12.4%, smaller in side length, reducing the effective buckling length that drives the truss member diameter. Using the sparse tessellation, each truss module has a hexagonal

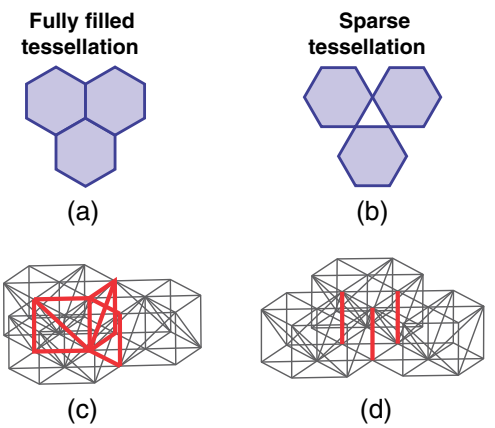


**Fig. 9** Top views of (a) fully filled and (b) sparse hexagonal tessellation. Hexagonal truss modules arranged in (c) fully filled and (d) sparse tessellations, with redundant members are shown in thickened red lines.

side length of 2.76 m and interfaces with its corresponding mirror module at the midpoint of the outer ring of mirror segments. The full primary mirror includes 270 DTMs forming nine rings around a central hexagonal hub. This hub is a monolithic unit including attachment points for the primary mirror solar array and docking points for the formation flying units during assembly and transit to SEL2. The innermost ring of six modules may be attached permanently to the hub to aid the initial assembly process. Mirror modules are attached to DTMs in the second ring out to the ninth ring.

We selected carbon fiber M55J tubes to be the primary material for the DTM based on its performance as a high modulus fiber. Following a published rationale for defining structural requirements for telescopes,[70] a minimum fundamental frequency requirement of 0.69 Hz was imposed on the backplane truss in order to achieve a dynamic surface precision of 1 $\mu$m, based on approximation to a plate-like structure. A design that satisfies the fundamental frequency requirement is a 2.76-m deep truss with that are a constant 45-mm diameter and 3-mm thick.[71] The end-beam hinges in each DTM can be passive pin-and-barrel hinges with no need for latching. However, the mid-beam hinges associated with the folding diagonals and longerons are ideally spring-loaded and latching hinges with high stiffness once deployment is complete. A preliminary trade study concluded that tape-spring hinges[72,73] would best satisfy the need for a latching hinge, compared to more complicated mechanisms, such as a snap-action or wedge latch. Tape-spring hinges for deployable booms have had flight heritage on Mars Express.[74] While the Mars Express booms experienced an incomplete deployment that was eventually resolved,[75] the assistance of the robotic system during deployment will provide robustness to any deployment anomalies. The fundamental frequency for this design is 1.1 Hz, exceeding the 0.69 Hz requirement, and achieving a structural areal density of 3.8 kg/m$^2$ considering only the truss members. This results in a backplane structural mass of $2.0 \times 10^4$ kg and a primary mirror total mass of $1.3 \times 10^5$ kg, which exceeds the $1.05 \times 10^5$ kg payload mass capacity of an SLS Block 1B vehicle to low Earth orbit (LEO).[60]

In order to conform to the 800-m radius of curvature of the primary mirror surface, the truss is designed with clearances that can be adjusted at the mechanical interconnects between DTMs. This is a benefit of the modular assembly, which allows all of the structural modules to be fabricated as identical units. The range of adjustability required in the DTM gaps based on the

AECT method, which was also used to position the mirror segments, is about 20 mm on the top and 35 mm on the bottom. This adjustability can be preset during the fabrication process or implemented by the robot during assembly. Each DTM includes fixtures on the top surface that provide gripping points and local fiducials to aid robotic mobility and to manage the process of unfolding the DTM using bimanual manipulation. The fiducials on the evolving frame help the robot maintain accurate knowledge of its current location.

### 4.4 *Formation Flying*

The telescope is separated into four formation-flying units. There are three levels of spacecraft control precision in this architecture. Fine (precise) formation control is only required between the primary mirror unit and the OIU using the relative sensing from the metrology unit, which must itself maintain medium-level control, and the sunshade requires only relatively coarse control to keep the primary craft in its shadow, as shown in Fig. 10. For operational practicality, flexibility, and robust design, a lead/follower formation architecture is used. In this scenario, the OIU, metrology unit, and sunshade are controlled relative to the much more massive primary mirror unit, which serves as the formation leader.

#### 4.4.1 *Orbital disturbance environment*

The formation is to operate in deep space about the SEL2 point, such as in a halo orbit. The prime advantage of a deep space location is the relatively benign dynamic environment and consequently lower fuel budget needed to maintain the formation. The primary disturbance for this relatively close formation is the differential SRP force. In deep space with hundreds of meters of separation between the key system elements, the differential gravity gradient forces are substantially less than SRP. Depending on the formation pointing relative to the sun, as illustrated in Fig. 10, the use of the sunshade greatly reduces (or removes) the differential SRP forces on the fine formation control of the telescope. To quantitatively evaluate the effect of SRP on the formation, Table 2 lists the SRP force acting on each craft. This analysis assumes a maximum surface area projected in the sun-line direction and a conservative SRP force based on a perfectly reflective body. To compensate for this constant SRP disturbance force, the required delta velocity ($\Delta V$) is computed per year. To stabilize an orbit at SEL2, an additional

**Table 2** Maximum SRP force (and equivalent acceleration in $\mu$g) acting on each spacecraft and consequent $\Delta V$ needed to maintain the formation.

| Spacecraft | Mass (kg) | Maximum surface area ($m^2$) | SRP force (mN) | $\Delta V$ (m/s per year) |
|---|---|---|---|---|
| Sunshade | 5000 | 7500 | 68.4 (1.368 $\mu$g) | 431.7 |
| Secondary | 15,000 | 150 | 1.37 (0.009 $\mu$g) | 2.88 |
| Metrology | 15,000 | 150 | 1.37 (0.009 $\mu$g) | 2.88 |

1 to 5 m/s per year for each craft is budgeted.[76] The total propellant capacity in a detailed design would scale based on the design lifetime of the telescope and on the availability of in-space refueling capability at the operational orbit.

#### 4.4.2 *Formation flying sensing and control*

The metrology design outlined in Sec. 4.2 is the sensing strategy used for the full six DOF spacecraft formation control. The laser gauge using the MSTAR technique is capable of relatively sensing both the primary and secondary craft axial displacements to 10 nm and transverse displacements with the camera down to 5 nm. The relative tip/tilt resolution is 0.14 and 2 nrad for the primary and secondary spacecraft, respectively.

The relative sensing from the dedicated metrology spacecraft dictates the capability of control achievable. By implementing a model predictive controller with the sensing given above, it is possible to control the spacecraft to tens of micrometers and $\mu$rad-level relative to the metrology unit. This level of precision achieved by the rigid body (spacecraft-relative) controller allows for the multilevel control scheme with rigid body mirrors and adaptive optics to achieve full wavefront control for imaging.

#### 4.4.3 *Propulsion*

To maintain a precise formation for visible imaging, it is necessary to have a propulsion system that is agile and precise as well as efficient. A suitable approach is to incorporate two propulsion systems, such as a multithruster chemical system for agile six DOF control and an efficient electric thruster for continuous disturbance rejection and translational slew maneuvers of the

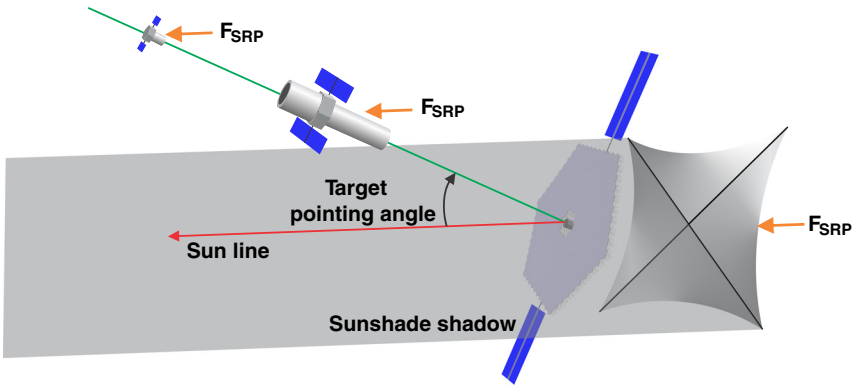


**Fig. 10** Inertial pointing of formation relative to sun line with SRP forces acting on each craft.

formation. As a quantitative example, the sunshade spacecraft with a 200 second specific impulse thruster would consume 1270 kg/year of fuel to compensate for SRP. Using the NASA Evolutionary Xenon Thruster (NEXT) with a 4170 second specific impulse[77] would consume 61 kg/year. For the much smaller (area) metrology spacecraft, the SRP compensation would consume 22 and 1 kg/year for the chemical propulsion system and NEXT ion thruster, respectively.

In the absence of a specific mission design and science expectations, a quantitative example of the fuel requirements for slew maneuvers to astronomical targets is the NWO starshade mission. This mission budgets 900 kg of fuel of xenon to be used by two NEXT thrusters to target 100 stars over a 5-year mission.[78] Further considerations on the propulsion and fuel usage for the telescope reference design include plume impingement concerns, which are vital with the close proximities and sensitive optics. For the sunshade to compensate the SRP force, it ideally thrusts with exhaust directly toward the primary mirror spacecraft. In reality, it is also necessary to consider exhaust plume impingement and the resulting degradation of optical elements and other sensitive components. To address this concern, the propulsion system will be implemented by canting multiple thrusters away from the direct line-of-sight between spacecraft, resulting in additional fuel consumption through cosine losses. The severity of this extra fuel required is dependent on the propulsion system and separation distance.

### 4.5 *Environmental Considerations*

In this section, we provide a brief overview of relevant effects from the space environment influencing the design and operation of the 100-m telescope. Specifically, thermal effects, the plasma and radiation environment, and meteoroid impacts can negatively influence the performance of the telescope.

A preliminary thermal analysis showed that rigid body actuators with a range of 10 mm are able to compensate for the change in primary mirror curvature resulting from a thermal gradient of over 13 K across the depth of the backplane truss.[71] Considering solar flux as the predominant external heat source at SEL2, a relatively low blockage factor of 0.6 is adequate to maintain a thermal gradient of under 7.5 K across the truss depth. Consequently, the sunshade design is driven primarily by stray light considerations.

The plasma and ionizing radiation environment at SEL2 includes effects from the solar wind and the geomagnetic tail as well as extrasolar sources of high-energy particles.[79] The sunshade will limit optical degradation of the primary mirror surface from solar wind ions; simulations with 4 keV protons and 16 keV alpha particles showed no penetration beyond 400 nm into a membrane consisting of 100 nm of aluminum and 2 $\mu$m of Kapton.[80] Electronic systems require shielding to limit total ionizing dose and prevent electrical discharge events.

Meteoroid bombardment will also erode the primary mirror surface, resulting in reduced optical throughput and degraded optical PSF. Impacts are dominated by small meteoroids, with no impacts expected from meteoroids larger than 3 mm and only 50 to 100 impacts between 1 and 3 mm over 5 years, based on a model of total interplanetary meteoroid flux at 1 AU.[81] Impacts resulting from meteoroid streams[82] are not expected to exceed the impact rate from the sporadic population for these small meteoroids. The cumulative impact area over 5 years is ~0.2% of the total surface, assuming no replacement of damaged mirror segments through robotic servicing. This estimated degradation is conservative and can be mitigated through operational strategies, for example, by limiting the duration that the primary mirror is facing directions with high meteoroid flux, such as the heliocentric orbital velocity direction.

## 5 Robotic System

The primary mirror is assembled by a six-limbed robot henceforth referred to as a hexbot. This robot will deploy and assemble the truss modules, attach the mirror modules onto the assembled truss, and remain with the telescope to perform servicing tasks, such as replacing individual mirror segments or electronics units. When not in operation, the hexbot will remain attached to the central hub of the primary mirror to await future servicing tasks.

### 5.1 *Hexbot Architecture and Requirements*

The hexbot architecture draws lineage from a number of robotic systems developed at JPL over last decade or more such as the ATHLETE and LEMUR robots.[83,84] The JPL RoboSimian robot that competed in the DARPA robotic challenge has some aspects of its design derived from this architecture.[85] It is conceptualized as a six-limbed robot with each limb having seven DOF. Similar to RoboSimian, these limbs can be constructed as a kinematic chain of identical modular rotational joints, with six DOF for determining the position and orientation of the end effector and a seventh DOF providing kinematic redundancy. The length of each limb segment can be scaled to effectively satisfy any reach requirement. The chassis is symmetric and sufficiently large to either carry a magazine with the folded DTMs or a mirror module.

To maintain a stable hold on key components, such as truss modules, dual handed manipulation[86,87] is expected to be required for many steps in the assembly process. To construct an optical quality structure, the error estimates point to about a centimeter level accuracy required for the manipulations involved in placing a module element within the evolving truss structure. This in turn requires a roughly 0.5-deg accuracy on the control of the orientation of the fully deployed truss modules. While a single hand can adequately maintain a safe grasp of a truss module, the positioning requirements for truss docking and assembly dictate the use of two hands. The robot can readily deploy the DTM from its compressed state to its fully operational state, as spring-loaded DTM hinges provide forces that unfold the DTM, and the fixtures on the DTM (Sec. 3.2) provide grasping points for the hexbot to manage the unfolding process. The hexbot's two-handed grip on the DTM then enables the positioning of the deployed DTM, or the mirror module, at its appropriate docking position on the truss work. Figure 11 shows a motion study demonstrating the dexterity of the hexbot. Docking cones or fiducials[88] on the DTM reduce the robot's required manipulation accuracy. Once one feature of the DTM is anchored to the main truss, the robot can use one of its free limbs to activate/assemble the structural and power interconnects that attach the DTM to the trusswork. Subsequent maneuvers, possibly guided by additional fiducials, will attach the DTM to the truss at multiple points.

The use of the gripping features on the DTMs/truss simplifies the complexity of the robot's end-effector. The same gripper can be used for unfolding and docking the DTMs, as well as walking over the truss using the designated grasping features. In the

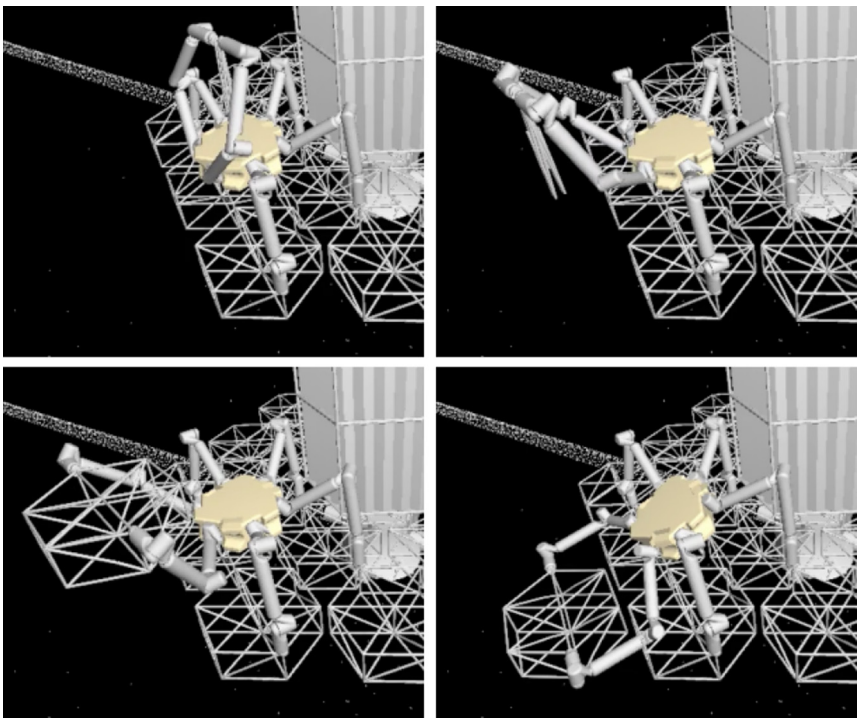

**Fig. 11** Conceptual CAD rendering of hexbot motion sequence as it deploys a DTM and positions it on the backplane.

worst case, a separate gripper, which can be retrieved from a tool change-out cartridge mounted on the robot's chassis (such as used in the Dextre robot[18]), might be needed for the mirror transport and attachment process. During assembly, the end-effectors also provide the actuation of the mechanical and electrical interconnects. The end-effectors can also be equipped with additional functions such as a probe to provide health data on the electrical system of the telescope.

The hexbot will use identical limbs that are capable of both manipulation and mobility operations. This approach is particularly suitable for on-orbit operations for which the mobility problem can be cast as a special case of manipulation. Moreover, each joint within the limb will use an identical drive-train. The JPL RoboSimian system,[85] whose legs are constructed from identical seven DOF modules, has demonstrated that such designs are viable and cost-effective. Particularly in space, where gravitational loading is not a constraint on robot design, such modular design approaches are feasible. Moreover, significant cost savings are possible, particularly for flight applications for which verification, validation, and acceptance tests are major cost drivers.

The gross motion planning algorithms will exploit the availability of multiple manipulators and actuation redundancy. In particular, mobility and manipulation tasks will be planned with contact points and orientations to minimize loads into the structures. As a simple example, with at least three points of contact at any one time, the loads on the trusswork can be planned to minimize reaction moments and emphasize reaction forces.[89] Forces can be reacted with much more structural efficiency than moments. Similarly, maneuvers that minimize rapid changes in the robot's center of mass displacement can also be enabled by the large number of robot DOF.[90]

Nearly axisymmetric limbs and omnidirectional visual sensor coverage makes perception and available actions indifferent to the heading of the robot. Because the robot does not need to reorient to see, move, or manipulate, energy- and time-efficiency are dramatically improved. The robot will use multiple pairs of stereo cameras on the chassis for navigation and situational awareness. Additional cameras mounted in the hand can provide assistance with the grasping and docking operations, and force–torque sensors at the distal end of each arm provide the measurements needed to manage the control of the internal forces within the truss-robot mechanism and to ensure that excessive assembly forces are not generated.[91] The hexbot's perception system is responsible for building, maintaining, and processing 3-D maps based on the stereo range images and visual odometry. The outputs of the perception system are used by the robot to plan collision-free motions, insertion of objects, and inspection of the environment.

We envision that the assembly interactions with the DTMs or mirror modules are controlled using hybrid position-force control techniques, such as the generalized compliant motion method.[92] Robotic assembly in space will require simultaneous force control and Cartesian trajectory tracking for module docking, dithering (random searching motions, e.g., for aligning a DTM with its neighbor before they are attached), and kinematic constraint satisfaction. Visual servoing[93] (the process of minimizing visual tracking errors by using visual feedback) will also be required during the docking, transportation, and module deployment processes to overcome errors and to manage assembly in the face of small manufacturing errors. Figure 12 shows photos of an experiment demonstrating force-controlled deployment of a DTM using dual-handed manipulation on the Surrogate robot at JPL.[94] This robot has two seven DOF arms mounted on a seven DOF torso. It incorporates force sensing wrists and a stereo vision system, as would be used for in-space robotic assembly. This experiment demonstrated that a combination of visual servoing, compliant motion

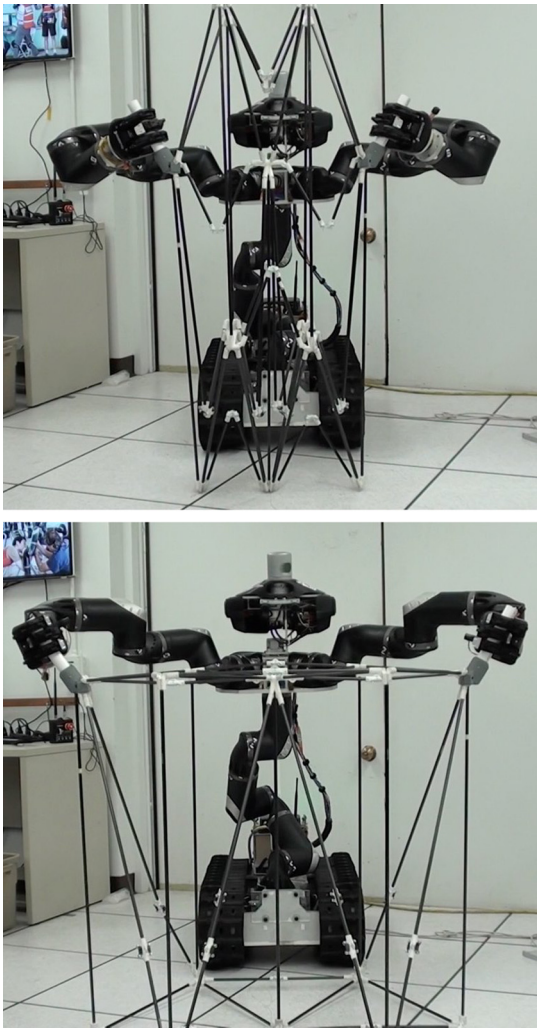

**Fig. 12** Laboratory demonstration of surrogate robot deploying a 1-m Pactruss module.

control, and bimanual manipulation coordination can enable a dual arm robot to deploy a space truss module, even in the presence of manufacturing tolerances.

### 5.2 *Assembly Sequence*

Robotic assembly of the primary mirror will be performed in Earth orbit to reduce the total mass that must be transported to SEL2. Additionally, communication from Earth orbit has lower latency and would enable more effective supervision of robotic operations. Based on the expected volume of the packaged DTMs and mirror modules, at least four SLS Block 1B launches will be required to transport all telescope components to orbit, with a potential manifest outlined in Table 3. These launches would be volume constrained if assembly occurs in LEO, but may be mass-constrained for a medium to high Earth orbit. The overall launch sequence would depend substantially on programmatic constraints, such as funding and launch facility availability.

The hexbot, primary mirror hub, and metrology unit are launched with the first payload of DTMs. The hexbot deploys and assembles the DTMs in rings around the primary mirror hub with feedback from the metrology unit to provide the required shape accuracy. The assembly of each DTM includes unfolding, coarse positioning, initial capture and docking with the assembled truss, adjustment to correct for geometric misalignments, and attachment of electrical power and data connections. Subsequent launches rendezvous with the primary mirror and dock a cargo housing unit to the hub, as illustrated in Fig. 3, providing additional DTMs followed by the mirror modules. Once the truss is complete, the mirror modules are attached in rings from the outside in, so that traversal of the robot over the region of assembled mirror segments is minimized. With feedback from the metrology unit, the mirror segment positions are adjusted using rigid body actuators. Payload support fixtures used to contain the DTMs and mirror modules for launch can then be discarded. Finally, the OIU and sunshade are launched and docked with the primary mirror. The metrology unit also docks temporarily to the mirror during transit to SEL2.

Upon arrival at SEL2, the separate formation flying units undock from the primary mirror and assume their operational configuration. The sunshade is deployed and the primary mirror is allowed to thermally stabilize. The metrology unit is used to verify and adjust the mirror segment positions, followed by full system verification and commissioning.

**Table 3** Possible component manifest by launch vehicle with mass estimates.

| Launch vehicle | Component | Mass (tons) |
|---|---|---|
| 1 | Hexbot | 2 |
| | M1 spacecraft | 10 |
| | Metrology spacecraft | 10 |
| | 45 mirror modules | 5 |
| | 40 truss modules | 21 |
| | **Total** | **48** |
| 2 | 90 truss modules | 10 |
| | 80 mirror modules | 42 |
| | **Total** | **52** |
| 3 | 90 truss modules | 10 |
| | 80 mirror modules | 42 |
| | **Total** | **52** |
| 4 | 45 truss modules | 5 |
| | 40 mirror modules | 21 |
| | Sunshade | 10 |
| | OIC | 20 |
| | Upper stage | 10 |
| | **Total** | **66** |

## 6 Conclusion

The key features of the RAMST architecture—deployable modules, advanced metrology, and robotic assembly—enable the realization of large-space telescopes by overcoming the mass

and volume constraints of launch while leveraging the economies of mass production to avoid exorbitant cost. The scalable nature of the architecture provides a straightforward path for technology development. While a 100-m telescope design is presented here, the RAMST architecture can be readily applied to smaller configurations; for example, a 10- to 20-m telescope launched only using secondary payload opportunities. Such a precursor mission would be essential for proving out the technologies required for the larger telescopes and would already provide a substantial increase in performance compared to any space telescopes in the near future.

## Acknowledgments

The research was carried out in part at the Jet Propulsion Laboratory, California Institute of Technology, under a contract with the National Aeronautics and Space Administration. K. Hogstrom was supported through this work by NASA Space Technology Research Fellowship #NNX13AL67H. N. Lee was supported through this work by a postdoctoral fellowship from the W. M. Keck Institute for Space Studies. The authors thank G. Malakhova and M. Cheung for their participation in the development of CAD models and DTM prototypes.

## References

1. P. A. Sabelhaus and J. E. Decker, "An overview of the James Webb Space Telescope (JWST) project," *Proc. SPIE* **5487**, 550–563 (2004).
2. Association of Universities for Research in Astronomy, *From Cosmic Birth to Living Earths: The Future of UVOIR Space Astronomy*, Washington, DC (2015).
3. M. Postman et al., "Advanced technology large-aperture space telescope: science drivers and technology developments," *Opt. Eng.* **51**(1), 011007 (2012).
4. L. D. Feinberg et al., "Modular assembled space telescope," *Opt. Eng.* **52**(9), 091802 (2013).
5. M. Johns et al., "Giant Magellan Telescope–overview," *Proc. SPIE* **8444**, 84441H (2012).
6. J. E. Nelson, T. S. Mast, and S. M. Faber, "The design of the Keck Observatory and Telescope," Technical Report Keck Observatory Report No. 90, Caltech (1985).
7. J. Nelson and G. H. Sanders, "TMT status report," *Proc. SPIE* **6267**, 626728 (2006).
8. European Southern Observatory (ESO), The E-ELT construction proposal, Technical Report (2011).
9. V. L. Krabbendam et al., "Development and performance of Hobby–Eberly Telescope 11-m segmented mirror," *Proc. SPIE* **3352**, 436–445 (1998).
10. R. Stobie, J. G. Meiring, and D. A. H. Buckley, "Design of the Southern African Large Telescope (SALT)," *Proc. SPIE* **4003**, 355–362 (2000).
11. European Southern Observatory (ESO), "OWL concept design report: phase A design review," Technical Report OWL-TRE-ESO-0000-0001 (2005).
12. J. J. Rey et al., "A deployable, annular, 30m telescope, space-based observatory," *Proc. SPIE* **9143**, 914318 (2014).
13. G. Durand et al., "TALC: a new deployable concept for a 20m far-infrared space telescope," *Proc. SPIE* **9143**, 91431A (2014).
14. J. L. Domber, P. Atcheson, and J. Kommers, "MOIRE: Ground test bed results for a large membrane telescope," in *AIAA SciTech Space Structures Conf.*, National Harbor, Maryland (2014).
15. J. Watson et al., "A history of astronaut construction of large space structures at NASA Langley Research Center," in *IEEE Aerospace Conf. Proc.*, Vol. 7, pp. 3569–3586 (2002).
16. W. Doggett, "Robotic assembly of truss structures for space systems and future research plans," in *IEEE Aerospace Conf. Proc.*, Vol. 7, pp. 7-3589–7-3598 (2002).
17. W. Bruner, C. Enriquez, and S. Thampi, "Mechanism analysis and verification approach for ISS truss assembly," in *37th Aerospace Mechanisms Symp.*, Johnson Space Center (2004).
18. E. Coleshill et al., "Dextre: improving maintenance operations on the international space station," *Acta Astronaut.* **64**(9), 869–874 (2009).
19. C. Joppin and D. Hastings, "On-orbit upgrade and repair: the Hubble Space Telescope example," *J. Spacecr. Rockets* **43**(3), 614–625 (2006).
20. C. Underwood et al., "Using CubeSat/micro-satellite technology to demonstrate the Autonomous Assembly of a Reconfigurable Space Telescope (AAReST)," *Acta Astronaut.* **114**, 112–122 (2015).
21. R. Muller, "Robotic assembly of a 20-meter space telescope," in *Ultra Lightweight Space Optics Challenge Workshop*, Napa, California (1999).
22. R. M. Muller, "Assembly and servicing of a large telescope at the International Space Station," in *IEEE Aerospace Conf. Proc.*, Vol. 7, 3611–3619 (2002).
23. S. K. Stephens and H. J. Willenberg, "Metrics for in-space telescope assembly techniques," in *IEEE Aerospace Conf. Proc.*, Vol. 8, pp. 3967–3977 (2003).
24. S. Basu, T. S. Mast, and G. T. Miyata, "A proposed autonomously assembled space telescope (AAST)," in *Space*, Long Beach, California (2003).
25. J. M. Hedgepeth, "Pactruss support structure for precision segmented reflectors," Technical Report NASA-CR-181747, NASA (1989).
26. G. Greschik and W. K. Belvin, "High-fidelity gravity offloading system for free-free vibration testing," *J. Spacecr. Rockets*, **44**(1), 132–142, (2007).
27. J. F. Shaker and T. H. Acquaviva, "Static stability of the Space Station solar array FASTMast structure," Technical Report NASA-TM-106895, NASA (1996).
28. D. Gross and D. Messner, "The Able deployable articulated mast—enabling technology for the Shuttle Radar Topography Mission," in *33rd Aerospace Mechanisms Symp.*, Pasadena, California (1999).
29. F. A. Harrison et al., "The nuclear spectroscopic telescope array (NuSTAR) high-energy X-ray mission," *Astrophys. J.* **770**(2), 1–19 (2013).
30. H. Sawada et al., "Mission report on the solar power sail deployment demonstration of IKAROS," in *52nd AIAA/ASME/ASCE/AHS/ASC Structures, Structural Dynamics and Materials Conf.*, Denver, Colorado (2011).
31. D. Alexander, P. Henderson, and G. Turner, "Advancements in large mesh reflector technology for multi-beam antenna applications," *IEEE 8th European Conf. on Antennas and Propagation*, pp. 410–412, The Hague (2014).
32. M. W. Thomson, "AstroMesh™ deployable reflectors for Ku- and Ka-band commercial satellites," in *20th AIAA Int. Communication Satellite Systems Conf. and Exhibit*, Montreal, Quebec, Canada (2002).
33. A. Meguro et al., "In-orbit deployment characteristics of large deployable antenna reflector onboard Engineering Test Satellite VIII," *Acta Astronaut.* **65**, 1306–1316 (2009).
34. Y. U. Cao, A. S. Fukunaga, and A. Kahng, "Cooperative mobile robotics: antecedants and directions," *J. Auton. Robots* **4**(1), 7–27 (1997).
35. L. E. Parker, "Multiple mobile robot systems," in *Springer Handbook of Robotics*, pp. 921–941, Springer Berlin, Heidelberg (2008).
36. V. R. Kumar and K. J. Waldron, "Force distribution in closed kinematic chains," *IEEE Trans. Rob. Autom.* **4**(6), 657–664 (1988).
37. E. Papadopoulos and S. Dubowsky, "Coordinated manipulator/spacecraft motion control of space robotic systems," in *Proc. IEEE Int. Conf. Robotics and Automation*, pp. 1696–1701 (1991).
38. J. H. Burge et al., "Design and analysis for interferometric measurements of the GMT primary mirror segments," *Proc. SPIE* **6273** (2006).
39. M. C. O'Neal and J. T. Spanos, "Optical pathlength control in the nanometer regime on the JPL phase-B interferometer testbed," *Proc. SPIE* **1542**, 359–370 (1991).
40. D. P. Scharf et al., "An overview of the formation and attitude control system for the Terrestrial Planet Finder formation flying interferometer," in *2nd Int. Symp. on Formation Flying Missions and Technologies*, Washington, DC (2004).
41. K. G. Carpenter et al., "The Stellar Imager (SI) project: a deep space UV/Optical Interferometer (UVOI) to observe the Universe at 0.1 milliarcsec angular resolution," *J. Astrophys. Space Sci.* **320**(1–3), 217–223 (2009).

42. D. Sirbu, C. V. Karsten, and N. J. Kasdin, "Dynamical performance for science-mode stationkeeping with an external occulter," *Proc. SPIE* **7731**, 773152 (2010).
43. W. Cash et al. "The new worlds observer: the astrophysics strategic mission concept study," *Proc. SPIE* **7436**, 743606 (2009).
44. D. P. Scharf, J. A. Keim, and F. Y. Hadaegh, "Flight-like ground demonstrations of precision maneuvers for spacecraft formations—Part I," *IEEE Syst. J.* **4**(1), 84–95, (2010).
45. D. P. Scharf, J. A. Keim, and F. Y. Hadaegh, "Flight-like ground demonstrations of precision maneuvers for spacecraft formations—Part II," *IEEE Syst. J.* **4**(1) 96–106, (2010).
46. D. P. Scharf et al., "Precision formation flying at megameter separations for exoplanet characterization," *Acta Astronaut.* (2016) (in press).
47. M. Delpech et al., "Flight demonstration of formation flying capabilities for future mission (NEAT pathfinder)," *Acta Astronaut.* **105**, 82–94 (2014).
48. J. S. Ardaens, R. Kahle, and D. Schulze, "In-flight performance validation of the TanDEM-X autonomous formation flying system," in *5th Int. Conf. on Spacecraft Formation Flying Missions and Technologies*, Munich, Germany (2013).
49. G. Bonin et al., "CanX-4 and CanX-5 precision formation flight: mission accomplished!" in *Proc. of the 29nd Annual AIAA/USU Conference on Small Satellites*, Logan, Utah (2015).
50. C. P. Mandy et al., "Implementation of satellite formation flight algorithms using SPHERES aboard the international space station," in *Int. Symp. on Space Flight Dynamics*, Annapolis, Maryland (2007).
51. J.S. Llorente et al., "PROBA-3: precise formation flying demonstration mission," *Acta Astronaut.* **82**, 38–46 (2013).
52. D. F. Woods, "Space surveillance telescope: focus and alignment of a three mirror telescope," *Opt. Eng.* **52**(5), 053604 (2013).
53. A. Meinel and M. Meinel, "Two-stage optics: high-acuity performance from low-acuity optical systems," *Opt. Eng.* **31**(11), 2271–2281 (1992).
54. G. Brusa et al., "MMT adaptive secondary: first AO closed loop results," *Proc. SPIE*, **5169** (2003).
55. T. R. Price and M. A. Ealey, "Adaptive tertiary mirror for segmented mirror control," *Proc. SPIE* **5166**, 157–164 (2004).
56. A. Wirth et al., "Deformable mirror technologies at AOA xinetics," *Proc. SPIE* **8780**, 87800M (2013).
57. J. Steeves et al., "Design, fabrication and testing of active carbon shell mirrors for space telescope applications," *Proc. SPIE* **9151**, 915105 (2014).
58. M. A. Ealey and J. A. Wellman, "Ultralightweight silicon carbide mirror design," *Proc. SPIE* **2857**, 74–77 (1996).
59. J. J. Rey et al., "A low cost, high performance, 1.2m off-axis telescope built with NG-Xinetics silicon carbide," *Proc. SPIE* **8146**, 81460N (2011).
60. National Aeronautics and Space Administration, "Space Launch System (SLS) Program Mission Planner's guide (MPG) executive overview," Technical Report SLS-MNL-201, NASA (2014).
61. N. Lee, S. Pellegrino, and Y.-H. Wu, "Design algorithm for the placement of identical segments in a large spherical mirror," *J. Astron. Telesc. Instrum. Syst.* **1**(2), 024002 (2015).
62. J. H. Burge, L. R. Dettmann, and S. C. West, "Null correctors for 6.5-m $f/1.25$ paraboloidal mirrors," in *Fabrication and Testing of Aspheres*, J. Taylor, M. Piscotty, and A. Lindquist, Eds., OSA Trends in Optics and Photonics, Vol. **24**, Optical Society of America, Washington, DC (1999).
63. O. Lay, "MSTAR: an absolute metrology system with submicrometer accuracy," *Proc. SPIE* **5491**, 1068–1078 (2004).
64. J. Wallace et al., "Phase-shifting Zernike interferometer wavefront sensor," *Proc. SPIE* **8126**, 81260F (2011).
65. R. Jensen-Clem, J. K. Wallace, and E. Serabyn, "Characterization of the phase-shifting Zernike wavefront sensor for telescope applications," in *IEEE Aerospace Conf.* (2012).
66. N. A. Massie, R. D. Nelson, and S. Holly, "High-performance real-time heterodyne interferometry," *Appl. Opt.* **18**(11), 1797–1803 (1979).
67. J. R. Fienup, "Phase retrieval algorithms: a comparison," *Appl. Opt.* **21**(15), 2758–2769 (1982).
68. D. S. Acton et al., "James Webb Space Telescope wavefront sensing and control algorithms," *Proc. SPIE* **5487**, 887–896 (2004).
69. J. M. Hedgepeth, "Evaluation of Pactruss design characteristics critical to space station primary structure," Technical Report NASA-CR-178171, NASA (1987).
70. M. S. Lake, L. D. Peterson, and M. B. Levine, "Rationale for defining structural requirements for large space telescopes," *J. Spacecr. Rockets* **39**(5), 674–681 (2002).
71. K. Hogstrom et al., "A robotically-assembled 100-meter space telescope," in *Int. Astronautical Congress, IAC-14-C2.2.6*, International Astronautical Foundation, Toronto, Canada (2014).
72. H. M. Y. C. Mallikarachchi and S. Pellegrino, "Deployment dynamics of composite booms with integral slotted hinges," in *50th AIAA/ASME/ASCE/AHS/ASC Structures, Structural Dynamics and Materials Conf.*, AIAA, Palm Springs, California (2009).
73. A. M. Watt and S. Pellegrino, "Tape-spring rolling hinges," in *36th Aerospace Mechanisms Symp.*, pp. 37–50, Cleveland, Ohio (2002).
74. G. W. Marks, M. T. Reilly, and R. L. Huff, "The lightweight deployable antenna for the MARSIS experiment on the Mars express spacecraft," in *36th Aerospace Mechanisms Symp.*, pp. 183–196, Cleveland, Ohio (2002).
75. D. S. Adams and M. Mobrem, "Lenticular jointed antenna deployment anomaly and resolution onboard the Mars Express spacecraft," *J. Spacecr. Rockets* **46**(2), 403–410 (2009).
76. R. J. Luquette, "New Worlds Observer formation control design based on the dynamics of relative motion," in *AIAA Guidance, Navigation and Control Conf.*, Honolulu, Hawaii (2008).
77. R. Shastry et al., "NASA's Evolutionary Xenon Thruster (NEXT) long duration test as of 736 kg of propellant throughput," in *48th AIAA/ASME/SAE/ASEE Joint Propulsion Conf.*, Atlanta, Georgia (2012).
78. S. W. Benson, A. S. Lo, and T. M. Glassman, "Solar electric propulsion for the New Worlds Observer terrestrial exoplanet mission," in *45th AIAA/ASME/SAE/ASEE Joint Propulsion Conf.*, Denver, Colorado (2009).
79. S. W. Evans, Ed., "Natural environment near the Sun/Earth-Moon L2 libration point," *Next Generation Space Telescope Program*, http://www.dept.aoe.vt.edu/~cdhall/courses/aoe4065/OtherPubs/SPECS/L2environment.pdf, 2002 (10 June 2015).
80. G. Vulpetti, *Fast Solar Sailing, Space Technology Library*, Vol. **30**, Springer, The Netherlands (2013).
81. E. Grün et al., "Collisional balance of the meteoritic complex," *Icarus* **62**, 244–272 (1985).
82. P. Jenniskens, "Meteor stream activity I: the annual streams," *Astron. Astrophys.* **287**, 990–1013 (1994).
83. .B. Wilcox et al., "ATHLETE: a cargo handling and manipulation robot for the Moon," *J. Field Rob.* **24**(5), 421–434 (2007).
84. T. G. Miller and S. Rock, "Control of a climbing robot using real-time convex optimization," *Mechatronics* **18**(5–6), 301–313 (2008).
85. B. W. Satzinger et al., "Experimental results for dexterous quadruped locomotion planning with RoboSimian," in *Proc. Int. Symp. on Experimental Robotics* (2014).
86. C. Smith et al., "Dual arm manipulation—a survey," *Rob. Autom. Syst.* **60**(10), 1340–1353 (2012).
87. P. Hebert et al., "Dual arm estimation for coordinated bimanual manipulation," in *Proc. IEEE Int. Conf. Robotics and Automation*, pp. 120–125 (2013).
88. G. E. Musgrave, A. M. Larsen, and T. Sgobba, Eds., *Safety Design for Space Systems*, Elsevier, Oxford, United Kingdom (2009).
89. S. P. Boyd and B. Wegbreit, "Fast computation of optimal contact forces," *IEEE Trans. Rob.* **23**(6), 1117–1132 (2007).
90. K. Shankar and J. W. Burdick, "Kinematics for combined quasi-static force and motion control in multi-limbed robots," in *Proc. IEEE Int. Conf. Robotics and Automation*, pp. 2963–2970, Hong Kong (2014).
91. P. Hebert et al., "Fusion of stereo vision, force-torque sensors, and joint sensors for estimation of in-hand object location," in *Proc. IEEE Int. Conf. Robotics and Automation*, pp. 5935–5941, Shanghai (2011).
92. P. Backes, "Generalized compliant motion with sensor fusion," in *Proc. IEEE Int. Conf. Robotics and Automation*, pp. 1281–1286 (1991).
93. S. Hutchinson, G. D. Hager, and P. I. Corke, "A tutorial on visual servo control," *IEEE Trans. Rob. Autom.* **12**(5), 651–670 (1996).
94. P. Hebert et al., "Supervised remote robot with guided autonomy and teleoperation (SURROGATE): a framework for whole-body manipulation," in *IEEE Int. Conf. on Robotics and Automation*, pp. 5509–5516 (2015).

**Nicolas Lee** is an engineering research associate in aeronautics and astronautics at Stanford University, after receiving his PhD at Stanford University and a W. M. Keck Institute for Space Studies postdoctoral fellowship at Caltech. His current research interests include space environmental monitoring, deployable space structures, and small spacecraft systems.

**Sergio Pellegrino** is the Joyce and Kent Kresa professor of aeronautics and professor of civil engineering at Caltech and a Jet Propulsion Laboratory Senior Research Scientist. He received a laurea in civil engineering from the University of Naples in 1982 and a PhD in structural mechanics from the University of Cambridge in 1986. His general area of research is the mechanics of lightweight structures, with a focus on packaging, deployment, shape control and stability.

**Kristina Hogstrom** is a PhD candidate in space engineering at Caltech and a NASA Space Technology Research Fellow. She holds an MS in space engineering from Caltech and a BS in mechanical engineering with a minor in astronomy from Boston University. Her research focuses on the behavior of deployable modules for robotically assembled space structures, such as large space-based optical reflectors.

**Carl Seubert** is a technical member of the Guidance and Control Analysis group at the NASA Jet Propulsion Laboratory (JPL). He manages the spacecraft formation control testbed, a unique laboratory dedicated to multidegree of freedom dynamic testing and technology development. Using high fidelity simulations and hardware in the loop testing, he designs autonomous guidance and control algorithms for missions ranging from spacecraft formation flight, planetary landing, and proximity operations at small bodies.

**Yen-Hung Wu** received an MS in optical engineering in 2007 from the University of Arizona. Since 2007, he has been a staff engineer at the Jet Propulsion Laboratory, California Institute of Technology. He is a member of the optical design and engineering group and was the optical and optomechanical engineer for the NuSTAR metrology laser.

Biographies for the other authors are not available.